CARAPACE: a novel Composite Advanced Robotic Actuator Powering Assistive Compliant Exoskeleton

Preliminary Design

Lorenzo Masia*[1], Leonardo Cappello[1],
Pietro Morasso[1]
[1]Robotics Brain and Cognitive Sciences Dept.
Fondazione Istituto Italiano di Tecnologia (IIT)
Genoa, Italy
Lorenzo.Masia@iit.it
Leonardo.Cappello@iit.it
Pietro.Morasso@iit.it

Xavier Lachenal[2], Alberto Pirrera[2], Paul Weaver[2]
[2]Advanced Composites Centre for Innovation and Science
University of Bristol
Bristol, UK
Xavier.Lachenal@bristol.ac.uk
Alberto.Pirrera@bristol.ac.uk
Paul.Weaver@bristol.ac.uk

Filippo Mattioni[3]
[3]Hengshen Carbon Fibre
Southampton, UK
Filippo.Mattioni@hscarbonfibre.co.uk

***Abstract*—a novel actuator is introduced that combines an elastically compliant composite structure with conventional electromechanical elements. The proposed design is analogous to that used in Series Elastic Actuators, its distinctive feature being that the compliant composite part offers different stable configurations. In other words, its elastic potential presents points of local minima that correspond to robust stable positions (multistability). This potential is known a priori as a function of the structural geometry, thus providing tremendous benefits in terms of control implementation. Such knowledge enables to overcome the complexities arising from the additional degrees of freedom associated with link deformations and uncovers challenges that go beyond those posed by standard rigid-link robot dynamics. It is thought that integrating a multistable elastic element in a robotic transmission can open new scenarios in the field of assistive robotics, as the system may help a subject to stand or carry a load without the need for an active control effort by the actuators.**

Keywords——Multistable composite Material, Novel Actuator, Assistive technology, Force and Admittance Control.

I. INTRODUCTION

In most advanced applications of robotic engineering, the design is focused on dimensioning rigid components, characterized by an inherently high structural stiffness. This is done in order to avoid any flexibility or deformation of the links while interacting or manipulating objects, and represents the main reason that slender components, such as beams, plates or shells, are usually not present in robotic devices.

In general, robotic designers avoid compliant structures because they may cause unwanted shape changes and result in the onset of structurally nonlinear regimes, which, in turn, may lead to catastrophic and often sudden, uncontrolled, failure.

Furthermore, control implementation of flexible robotics is still an open issue. The motivation for this work is to show that if we learnt to govern structural nonlinearities, they could actually be exploited to some benefits.

There are several examples of compliant structures used in the design of novel actuators or studies focused on the control of flexible link robots [1][2][3]. However, previous approaches were mostly focused on minimizing, rather than exploiting, elastic effects (especially nonlinear ones). This is, indeed, particularly important in applications where high position accuracy is a primary requirement. We mention, for instance, DC brushless actuators. Their advent has provided the best performance in terms of torque/weight ratio by introducing direct drive force control and eliminating friction and backlash that were typical of motors with transmissions. However, attempts to reduce nonlinear behaviors and inertia in this actuation technology have lead to an inevitable increase in mass and cost.

A solution was proposed with the introduction of Series Elastic Actuators [4][5]. Indeed, reducing the interface stiffness by inserting series elasticity at the interaction port between the electromechanical actuator and the load, can substantially decrease the peak output force and acts as low-pass filter [6][7], thus increasing the system safety. With such architecture, the force control problem can be addressed by a fine position control because the output force is directly related to the mutual distance between the load and the end effector across the series elasticity. Despite their diffusion, such kind of technology is still underexploited, especially for robotic applications where position accuracy is the primary requirement and structures' compliance results in errors of the effector's end and inefficiency in production line. On the other hand, for biomimetic applications [8-10] and human robot interaction [11], variable stiffness actuation remains the most

effective solution, allowing a fine modulation of the interaction force and also providing the possibility for energy storage due to the presence of elastic elements [12][13].

The purpose of the work presented here is to use a compliant architecture that, by merging different technologies (electromechanical and composite materials), aims at responding to different dynamic conditions by preserving the accuracy requirements for both force and position control. The main idea is to exploit flexible structures to develop *Compliant "Morphing" Mechanisms* [14-16] with embedded actuators to be integrated at joint level. In particular, here this is done utilizing the *Multistable Composite Structures* of the kind presented by Lachenal et al. [17] and Pirrera et el. [18-20] .

The foundational hypothesis for the CARAPACE system (see title for the acronym meaning) can be summarized as follows. Structural components in robotic systems are generally designed to be stiff and respond linearly to the stimuli arising from different operating regimes. However, allowing controlled, well-behaved, nonlinear deformations could enable stiffness tailoring, to adapt deformations and work constructively as an integrating part of the wider mechanism. In following sections, we propose a novel design based on the synthesis of electromechanical actuation and multistable composite materials. In the remainder of the paper, the multi-stability of the system is detailed, an admittance control is implemented and preliminary stability tests are performed.

II. Actuator Design

A. Mechanics of the actuation system

The actuator is comprised of an electromechanical system (brushless motor) and a multistable composite transmission (MCT) (Figure 1A) directly connected to the motor's shaft. The MCT is made of two pre-stressed flanges combined using stiff connecting spokes and it is able to take any twisted configuration between a coiled and a straight configuration. Figure 1A shows the MCT in the straight and twisted configuration (top and bottom illustration, respectively). When the motor shaft rotates one end of the MCT, the latter twists and assumes a helical shape that depends on the motor's rotation. The torque of the motor is then transformed into an axial force and the reduction ratio depends on the inclination of the flanges, as illustrated in Figure 1B. The following section details the analytical formulation for the MCT's strain energy assuming an inextensional model for the flanges' deformation. Expressions for the stable equilibria are derived for a MCT with specific fibre orientations (lay-up).

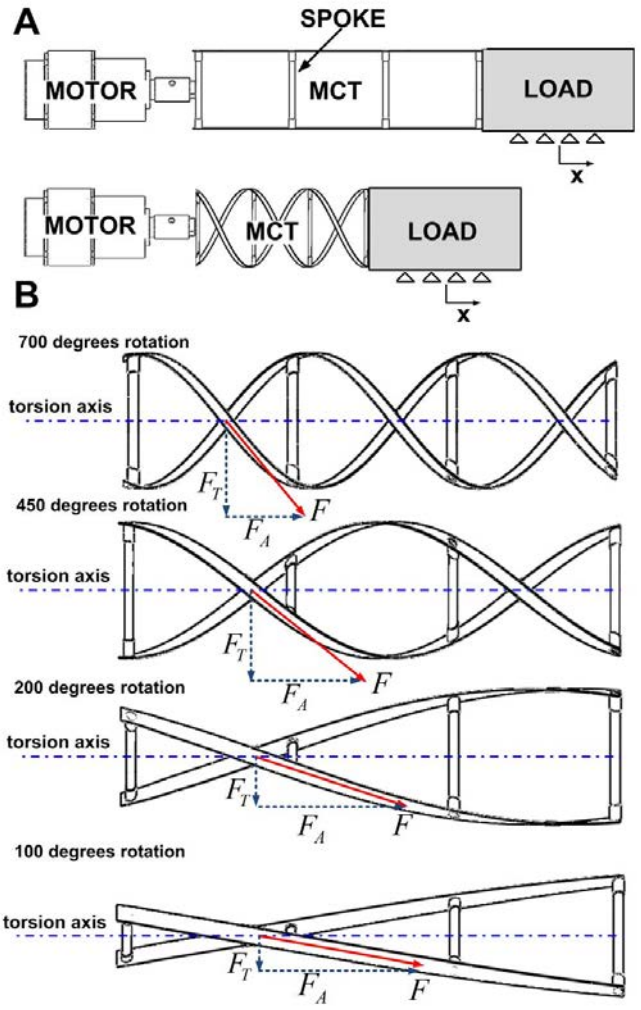

Fig. 1. A: A: assembly of the electromechanical actuator, the multistable composite transmission and the load. B: the MCT assumes different orientations of the flanges with increasing angular rotationand changes the axial force F_A trasmitted to the load.

III. MCT Analytical Model

A. Definition

The word lay-up describes the arrangement of the layers (plies) of composite material constituting a laminate. It is expressed as a series of numbers between brackets, defining the angles of the principal direction of each layer with regards to a reference axis. A lay-up is called symmetric when layers of the same properties, thickness and ply angle are positioned symmetrically with regards to the mid-plane of the laminate [21, 22]: $[\alpha/\beta/\chi/\chi/\beta/\alpha]$, where a Greek letter is used to indicate the ply angle. In this study, the lay-ups are limited to $[\beta/\beta/0/\beta/\beta]$ to reduce the design space.

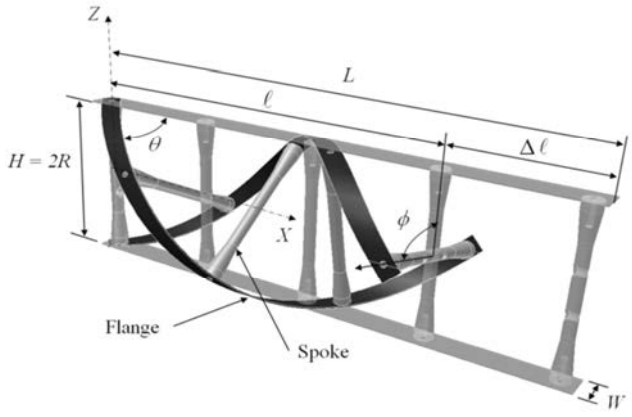

Fig 2. Sketch showing the structure in the straight (light grey) and twisted (black) configurations. The angle of helix θ and the constant height H of the structure are also shown.

B. Introduction and Assumptions

In the straight configuration, shown as light grey in Figure 2, the structure consists of two flat flanges kept apart by a set of rigid spokes. As mentioned earlier, the device can twist by applying opposite moments about the *X*-axis at the extremities of the structure, resulting in the configuration shown in black in Figure 2. The helix is multi-stable; i.e. it only needs energy to snap from one stable equilibrium to another. This is achieved by pre-stressing the flanges. The state of pre-stress simply results from manufacturing the parts on a cylindrical mould of radius R_i and flattening them for assembly of the MCT.

The work presented here draws upon modelling worked by Lachenal et *al*. [17]. The MCT behaviour is analysed through the evolution of its strain energy. Because the spokes keep the flanges at a constant distance throughout the transformation, we consider the flanges to lie tangential to an imaginary underlying cylinder of constant diameter equal to the spoke's length $H = 2R$, see Figure 2. Furthermore, because the flanges are narrow, we assume that their mid-surface does not stretch and deforms uniformly, i.e. the membrane strain energy associated with the twist of the MCT is neglected. These assumptions allow only two parameters to define every possible configurations of the structure; the curvature $1/R$ of the underlying cylinder and the orientation of the local axes (x,y) attached to each flange with respect to the axis of the cylinder, defined by the angle θ, as illustrated in Figure 2.

C. Strain Energy and Stable Equilibriums

As the transformations are assumed to be inextensional, the strain energy of one flange has the expression [21]

$$U = \frac{1}{2}\Delta\boldsymbol{\kappa}^{\mathrm{T}}\mathbf{D}^{*}\Delta\boldsymbol{\kappa} L W \,, \tag{1}$$

where L, W are the length and width of the flange respectively, the superscript $^{\mathrm{T}}$ denotes the transpose of the vector change of curvature $\Delta\boldsymbol{\kappa}$ (equation (3)) and $\mathbf{D}^{*} = \mathbf{D} - \mathbf{B}\mathbf{A}^{-1}\mathbf{B}$ is the reduced flexural stiffness of the flange as defined in classic lamination theory [22]. To find the stable equilibrium states of the structure, we look for points meeting the following two conditions; the first derivative of the strain energy with respect to θ is equal to zero and the second derivative of the strain energy with respect to θ is strictly positive

$$\frac{\partial U}{\partial \theta} = 0 \,, \; \frac{\partial^2 U}{\partial \theta^2} > 0 \,. \tag{2}$$

D. Curvature Change

The tensor $\Delta\boldsymbol{\kappa}$ describing the change of curvature can be found for any R and θ in the (x,y) coordinate system using a Mohr's circle of curvature [23]. In our case, the parts being manufactured on a curved tool of radius R_i, the initial curvature $\kappa_x = 1/R_i$ must be considered in the expression of the change of curvature; thus the ratio $\alpha = R_i/R$ relating the manufacturing radius R_i and the radius R of the underlying cylinder is defined. It is worth noting that the change of curvature across the width of the flange is not imposed by the geometry of the helix; instead it results from Poisson's ratio effects and is found by solving the equation of moment of the flange about the y-axis considering its free-edge boundary condition. Hence, the change in curvature to any configuration of a flange can be described by the vector $\Delta\boldsymbol{\kappa}$

$$\Delta\boldsymbol{\kappa} = \begin{bmatrix} \Delta\kappa_x \\ \Delta\kappa_y \\ \Delta\kappa_{xy} \end{bmatrix} = \frac{1}{2R}\begin{bmatrix} 1-\cos(2\theta)-\dfrac{2}{\alpha} \\ \dfrac{D_{12}^{*}}{D_{22}^{*}}\left(\cos(2\theta)+\dfrac{2}{\alpha}-1\right)-2\dfrac{D_{26}^{*}}{D_{22}^{*}}\sin(2\theta) \\ 2\sin(2\theta) \end{bmatrix}. \tag{3}$$

E. Strain energy tailoring

We now consider the stability of the structure as a function of the angle of helix θ and the $\mathbf{D}^{*}$ matrix of the flanges. Figures 3a and b are surface and contour polar plots, respectively, of the strain energy given by equation (1) for $\alpha = 2$, where the circumferential axis represents the angle of helix θ and the radial axis is the ply angle β. Note, that the flanges have dimensions $L = \pi \times R_i = 179$ mm by $W = 9$ mm in this numerical example. Peaks on the three dimensional surface plot correspond to unstable configurations whereas valleys indicate stable equilibria. Interestingly, the stable configurations rotate with increasing β, as shown in Figure 3b where the dotted lines represent the path of the stable configurations. As such, it is possible to create stable positions at any predefined helical angle by carefully choosing β, a feature that may be exploited the design of the present actuator. As an example, the points A…E correspond to stable positions for specific lay-up configurations $\beta = 0^{\circ}$, 45° and 180°.

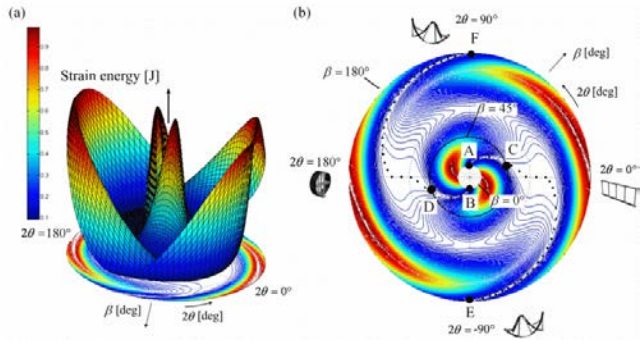

Figure 3. a. Surface representation and corresponding contour polar plot of *strain energy* as a function of 2θ and β for a structure made of a symmetric lay-up $[\beta/\beta/0/\beta/\beta]$, with a ratio $\alpha = 2$ and β ranging from 0° to 180°. b. Plan view of the same polar plot.

TABLE I: CFRP PROPERTIES [24].

Material	E_{11} [GPa]	E_{22} [GPa]	G_{12} [GPa]	ν_{12} [-]	ν_{21} [-]	t [mm]
8552/IM7	164	12	5	0.3	0.022	0.11*

*measured

F. Symmetric lay-up [45/45/0/45/45]

For the purpose of illustration we study the stability behavior of a MCT made of flange with a lay-up [45/45/0/45/45], and a ratio $\alpha = 2$ resulting in R = 28.5mm. The strain energy yielded by the device is shown in figure 4 as a function of the angle of helix θ. The points C and D shown in Figure 3b are also indicated in Figure 4.

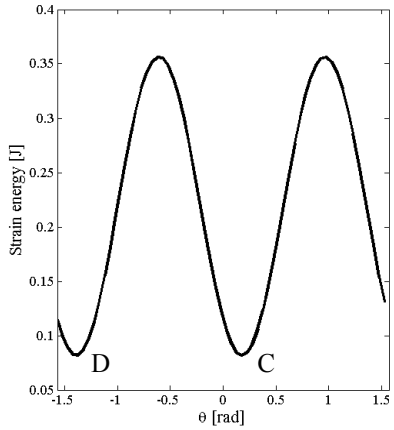

Fig 4. Evolution of the strain energy of the MCT for $-\pi/2<\theta<\pi/2$.

Applying Castigliano's theorem to the MCT, the axial force, stiffness, twist moment and torsional stiffness can be derived from equation (1), yielding:

$$F = \frac{\partial U}{\partial \Delta \ell}, \; k = \frac{\partial^2 U}{\partial \Delta \ell^2} \tag{4}$$

$$M = \frac{\partial U}{\partial \phi}, \; \Gamma = \frac{\partial^2 U}{\partial \phi^2} \tag{5}$$

where F, M is the axial force and twist moment applied to one end of the MCT respectively; k, Γ is the axial stiffness and torsional stiffness of the MCT respectively and $\Delta\ell$, ϕ are shown in Figure 2. The highly non-linear response of the MCT is shown by the plots of equations (4) and (5) as a function of θ in Figures 5a and 5b.

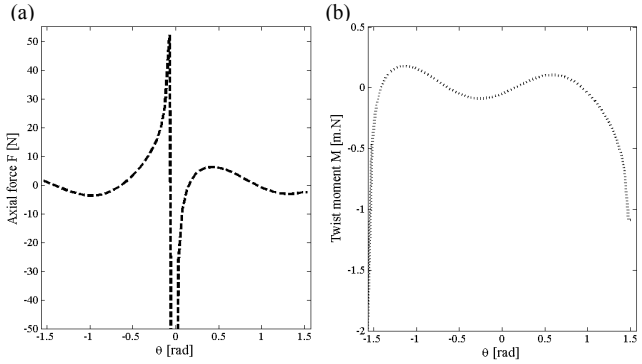

Fig 5. a. Axial force F and b. twist moment M for the MTC for $-\pi/2<\theta<\pi/2$.

IV. MODELING THE ACTUATOR

A. State Space Model

In order to understand the dynamic behavior of the proposed architecture, a model of the whole system comprising the electromechanical actuator and the multistable composite element with a lay-up [45/45/0/45/45] has been implemented as a two DoFs second order lumped system, see Figure 6.

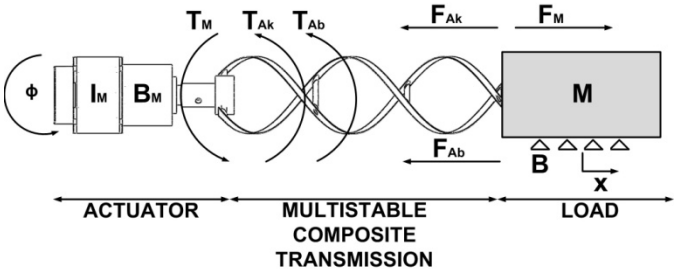

Fig 6. Assemlby of the entire system made by an elctromechanical actuator connected to the MCT and a load. Unitary mass of the load and inertia of the rotor are assumed for simplification and the MCT transmision is assumed to be massless but with an associated damping and stiffness.

The two masses correspond to the inertia of the rotor with the gear reduction and the load connected to the electromechanical actuator by the multistable composite transmission. By means of the latter component, the motion to the load is transmitted by a conversion of the angular rotation of the motor into a linear translation and the relationship between the two measures is highly dependent on the inclination of the helical shape of the carbon flanges during the motion. By observing Figure 7 it is clear that the ratio between the torque generated by the motor is also a function of the geometry of the multistable composite transmission. Hence, the force delivered to the load is a function of the helix angle, θ, with respect to the

axis of twist, which is the main parameter responsible for the conversion from torque to force. Considering the torque of the motor T_M and the radius of the helix R, the tangential force F_T can be written as:

$$F_T = \frac{T_M}{R} \tag{6}$$

To express the axial force delivered to the load, for a given θ, the following holds:

$$F_A = \frac{T_M}{R}\frac{\cos(\theta)}{\sin(\theta)} \tag{7}$$

In fact, for $\theta = 0$ a singularity arises as the MCT is in a completely extended configuration (F_A tends to infinity), while for $\theta = \pi/2$, the helix is in a coiled configuration, thus the axial force is equal to zero because the motor torque T_M is totally transformed in a tangential component F_T .

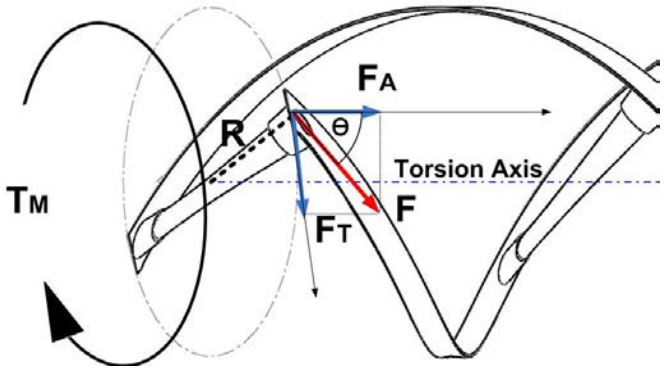

Fig 7. Components of the force trasmitted by the helical structure converting the torque deliverd by the eltromechanical actuator.

If we assume that the MCT is in one of the stable equilibrium configurations (point of local minimum of the strain energy), the dynamics of the two masses to simulate the behavior of the whole system for an impulse response are

$$\begin{aligned} M\ddot{x} + B\dot{x} &= F_M - F_{Ak} - F_{Ab} \\ I_M\ddot{\phi} + B_M\dot{\phi} + K_\tau\phi &= T_M - T_{Ab} \end{aligned} \tag{8}$$

where F_M is the axial force delivered by the motor to the load and corresponds to the force F_A of the equation 7, F_{Ak} and F_{Ab} are the restoring elastic force and the damping of the multistable composite element after it has been perturbed from its equilibrium position, respectively. While considering the electromechanical actuator delivering the torque T_M, there are also an elastic torque T_{Ak} and a damping T_{Ab} applied by the MCT on the rotor and counteracting the actuator's rotation to obtain the minimal energy configuration (equation 9).

$$\begin{aligned} T_{Ak} &= K_\tau\phi \\ T_{Ab} &= \frac{B_A \cdot ctg(\vartheta)}{Mr} \end{aligned} \tag{9}$$

By choosing the linear displacement of the load x and the angular rotation of the motor ϕ as state variables the state space representation of the two DoFs system is

$$\begin{aligned} \dot{X} &= A \cdot X + B \cdot u \\ Y &= C \cdot X + D \cdot u \end{aligned} \tag{10}$$

$$\dot{X} = \begin{bmatrix} 0 & 1 & 0 & 0 \\ -\frac{K_A}{M} & -\frac{B}{M} & 0 & -\frac{B_A \cdot ctg(\vartheta)}{Mr} \\ 0 & 0 & 0 & 1 \\ 0 & 0 & -\frac{K_\tau}{I_M} & -\frac{(B_M + B_A + B(\vartheta))}{I_M} \end{bmatrix} \cdot \begin{bmatrix} x \\ \dot{x} \\ \phi \\ \dot{\phi} \end{bmatrix} + \begin{bmatrix} 0 \\ \frac{ctg(\vartheta)}{Mr} \\ 0 \\ 1 \end{bmatrix} \cdot T_M$$

$$Y = \begin{bmatrix} 1 & 0 & 0 & 0 \\ 0 & 0 & 1 & 0 \end{bmatrix} \cdot \begin{bmatrix} x \\ \dot{x} \\ \phi \\ \dot{\phi} \end{bmatrix} + \begin{bmatrix} 0 \\ 0 \end{bmatrix} u$$

Assuming an open loop control scheme we may refer to a dynamic system of a unitary inertia I_M of the actuator and a unitary mass M of the load. By using this simplified model it is possible to simulate the behavior of the system for an impulse and observe the response of the oscillating masses of the rotor and the load. The MCT is made of carbon fiber which increases both damping and stiffness depending on the ply number and ply orientation (lay-up), as explained in the previous section. Assuming, for sake of simplicity, that the axial stiffness (K_A) is equal to the torsional one ($K\tau$) of the MCT, Table I reports different value of stiffness and damping used for simulating the response of the whole system.

TABLE I: VALUES OF THE STIFFNESS AND DAMPING OF THE MULTISTABLE COMPOSITE TRANSMISSION

MCT Simulated Stiffness (Kτ) and Damping (Bτ)	
K-B 1	K_A=Kτ=3200 N/m; B_A=20 Ns/m
K-B 2	K_A=Kτ =2000 N/m; B_A =15 Ns/m
K-B 3	K_A=Kτ =1500 N/m; B_A =12 Ns/m
K-B 4	K_A=Kτ =1000 N/m; B_A =10 Ns/m
K-B 5	K_A=Kτ =500 N/m; B_A =5 Ns/m

If the system is perturbed by a torque impulse sent by the electromechanical actuator the response will be different depending on the composition of the MTC. As we are not considering a closed but an open loop control, the overall behavior will result in an asymptotically stable second order damped oscillation. The results depicted in Figure 8 report an oscillation varying its shape depending on the stiffness and damping of the MCT. First, assume that the zero position of both the motor and the load corresponds to a configuration of

equilibrium of the MCT. Then, the response of the overall system consists of an oscillation around the equilibrium configuration because of the elastic behavior of the MCT trying to recover into its stable position with a restoring axial force.

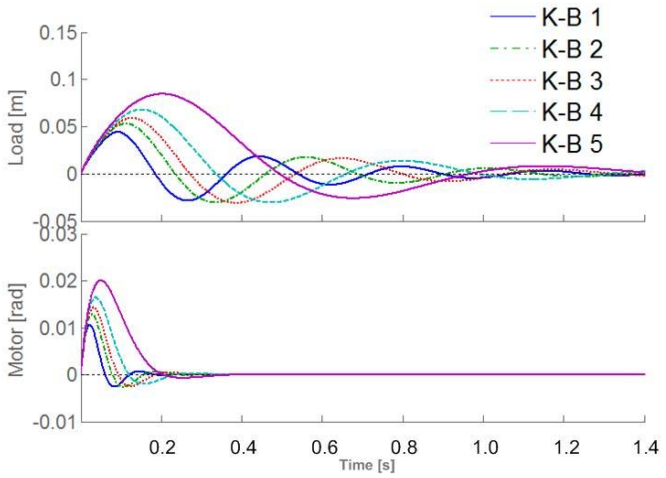

Fig 8. Response of the system to an impulse on on the motor torque. As depicted in the figure the response is more prompt for high stiffness and high value of damping of the MCT.

It is worth noting that a higher stiffness and damping (K-B 1) facilitate a prompt response of the system limiting the overshoot and decreasing the oscillations. The bode plot (Figure 9) depicting the transfer function and the phase of the system assuming as input the torque of the motor T_M and as output the displacement of the load X shows that for higher stiffness and damping (K-B 1), the bandwidth increases and the phase lag is significantly reduced. However, for lower values of the parameters (K-B 5), the bandwidth of the system is lower and the phase lag becomes apparent for lower frequencies.

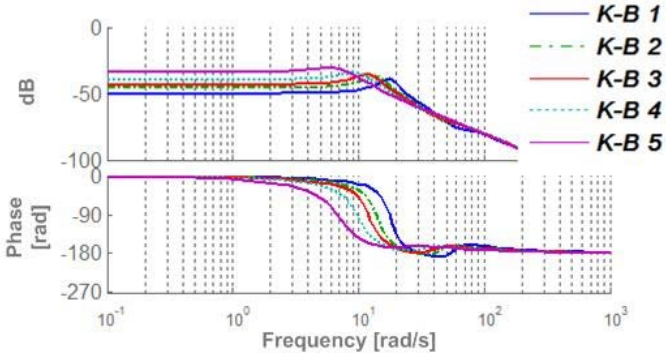

Fig 9. Bode plot of the tranfer function of the system evaluated considered in simulation the displacement of the load when the motor applies a torque.

V. EXPERIMENTAL CHARACTERIZATION

A. Closed loop control of the actuator

A test bench for characterizing the actuator was built. The structure comprises a brushless motor (Maxon ECi 40 70W and a 14:1 gearhead) connected to a MCT in symmetric lay-up [β/β/0/β/β] with β=45 degrees and a uniaxial force sensor (Futek LCM300 100lb capacity) that was used to implement a force control scheme (Figure 10A).

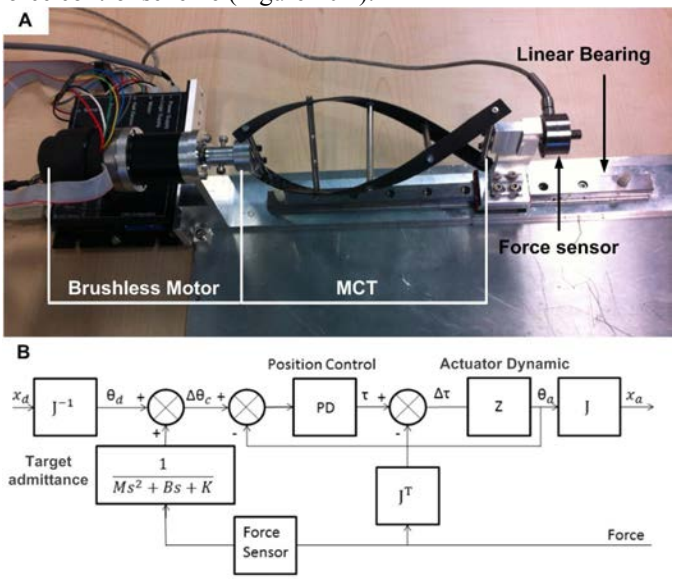

Fig 10. A: test bench made by the brushless motor, the MCT and the force sensor with a linear bearing.B:Admittance control scheme.

To test the system in closed loop we implemented an admittance control scheme (Figure 10B), consisting of two nested control loops. In the outer loop, the human-generated force, provided by a force sensor, is translated into a robot movement through a 'target admittance' block, which specifies the desired behavior of the actuator at the interface with the subject. In other words, the target admittance reflects the desired haptic rendering behavior and generates a desired device position. The inner loop is a PD position controller and is used to compensate for the intrinsic robot dynamics. By modifying the parameter *M, B, K* of the target admittance it is possible to impose different mechanical response to position step perturbation.

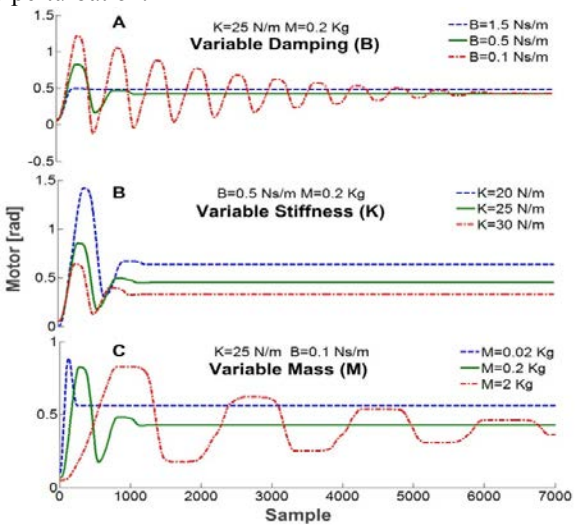

Fig 11: different trials observing step responses of the actuator when a 0.4 radians perturbation to the motor is imposed changing the admittance gains

Figure 11 depicts different behaviors of the actuator showing the rotation of gearhead connected to the MCT when a position perturbation is superimposed. It is important to note that the system, starting from one of its multiple equilibrium configurations (Figure 12), behaves as a non linear spring, trying to reconfigure to a minimum strain energy state after a displacement is applied: configurations of equilibrium for the used lay-up [β/β/0/β/β] with β=45°, are depicted in Figure 12 and evaluated by our mathematical model in Figure 3. The presence of the admittance controller fully compensates for the restoring force by superimposing the simulated dynamic (*M, B, K)* which is input to the inner position control loop as depicted in figure 10B and then feedback by the servo to drive the electromechanical actuator.

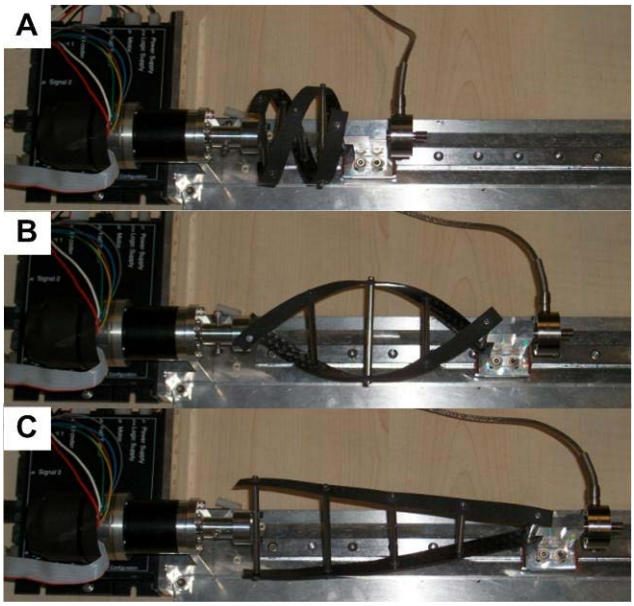

Figure 12: different configuration of equilibrium for the MCT used in the present setup with symmetric lay-up [45/45/0/45/45]. A-C: stable configurations of minimum strain energy. B: unstable configuration of maximum strain energy.

This approach is suitable when elastic deformation of the whole actuator is detrimental for specific operations. Then, it must be compensated for in order to have a higher accuracy in position and force control, mostly relying on the force detection at the tip of the sensor connected to the final part of the MCT. But, as stated in the introduction of the present work, well-behaved nonlinear deformations could enable structural stiffness tailoring to match different operating conditions. The capacity of MCTs to take multiple configurations of stable equilibrium, across their operating range, is a feature which will be result in major benefits, especially in those conditions when a robust holding position control is required. For example, assume a mechanism must hold a specific configuration rejecting disturbances. If such a configuration is close to the one local minimum of the MCT, then the control effort of the electromechanical counterpart can be relieved, instead relying on the intrinsic elasticity and damping ability of the MCT, which will be able to recover a stable configuration after an unexpected perturbation occurs.

Figure 13 shows a simple test where two admittance controllers were tested for a force input by a human acting directly on the force sensor and moving the actuator remotely from an equilibrium configuration of equilibrium (minimum of strain energy) In Figure 13.B, the red plot corresponds to the axial force applied by the human to the force sensor. The displacement (blue trace) is then evaluated by the admittance control and fed back to the motor as indicated on the top of Figure 13.B: when at the time T_1 the operator releases the force sensor the restoring force of the MCT should move the whole actuator back to the initial unperturbed configuration. In fact, once released the system remains in the perturbed configuration due the presence of the proportional action *K* of the *admittance control,* chosen to compensate for the elasticity of the MCT (clearly shown in figure 13.B). In Figure 13.A the situation changes, because the *admittance control* is now implemented to simulate a mass *M* and damping *B* and no proportional *K* gain is present. In this dynamic condition, at time T_1 the MCT applies a restoring force in order to reconfigure towards the minimum strain energy geometry before the perturbation was applied.

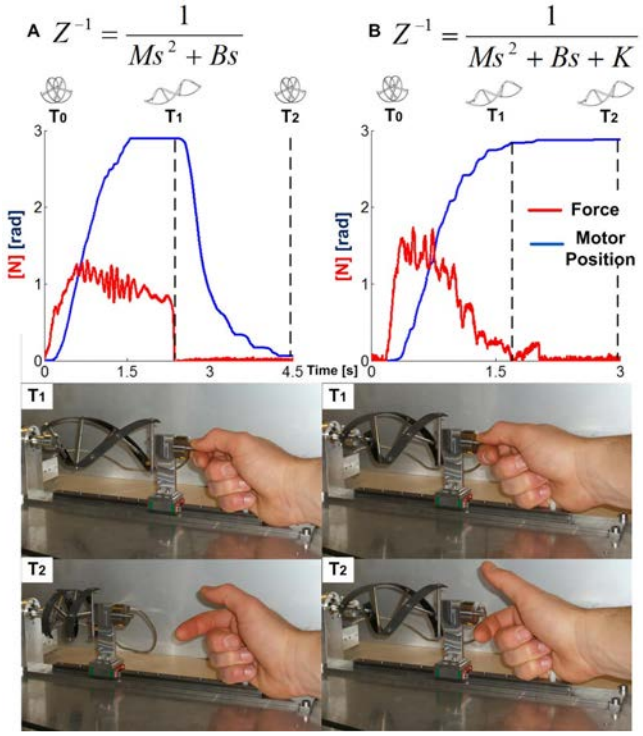

Figure 13: admittance test perturbing the actuator by a pulling force and releasing it. Right Panel: When the admittance control compensates for the elasticity of the MCT the system remains in the stretched configuration after the force applied by the human operator is removed. Left Panel: if the admittance control does not compensate the elastic behavior of the MCT the restoring force reconfigures the actuator to a minimum strain energy geometry

VI. DISCUSSION

In this paper, we introduced a novel actuation system comprised of multistable composite materials and

conventional electromechanical actuators. Merging these technologies can provide significant benefits to many robotic applications and especially to assistive robotics. The proposed actuation system follows the same philosophy of SEAS, which is based on the assumption that elastic deformation at the end effector can improve the safety and the accuracy of the actuator by filtering disturbances and hence preventing unexpected dynamic responses.

Multistable composite materials provide several advantages with respect to the simple elastic elements used in SEAS. Among others: they are lightweight and their dynamic behavior can be accurately modeled and tailored to target different applications.

These unique features can be exploited to elegantly address problems such as:

- the dynamic compensation of moving elements in a mechanism, by superimposing a geometry-dependent force;
- the realization of energy saving/harvesting systems, by allowing the MCT to compensate/absorb and consequently feedback the oscillations generated by the inertial dynamics (especially in cases where the position control is continuously required to solve a repetitive task, e.g. a production line);
- the realization of lightweight assistive support devices exploiting the MCT's multiple equilibrium configurations. An example of this could be a load-carrying exoskeleton, in which, differently from conventional systems, the load is resisted by the blocking force of one of the MCT's equilibrium configurations, rather than by the power of an electromechanical actuator.

These points will be the subject of future research.

ACKNOWLEDGMENT

The work is a collaboration between Robotic Brain and Cognitive Science Dept of Istituto Italiano di Tecnologia and ACCIS Advanced Composites Centre for Innovation and Science, University of Bristol.

REFERENCES

[1] *De Luca, W. Book, "Robots with Flexible Elements," in Springer Handbook of Robotics, B. Siciliano, O. Khatib (Eds.), pp. 287-317, Springer Verlag, Berlin, 2008.*

[2] *A. De Luca, P. Lucibello, "A general algorithm for dynamic feedback linearization of robots with elastic joints," 1998 IEEE International Conference on Robotics and Automation, Leuven, B, pp. 504-510, 1998*

[3] *A. Albu-Sch¨affer, Ch. Ott, and G. Hirzinger, "A unified passivity based control framework for position, torque and impedance control of flexible joint robots," The Int. J. of Robotics Research, vol. 26, no. 1, pp. 23–39, 2007.*

[4] *G. A. Pratt and M.M. Williamson, Series Elastic Actuators, Intelligent Robots and Systems 95. Human Robot Interaction and Cooperative Robots, 1995.*

[5] *G. A. Pratt and M. M. Williamson, ''Series elastic actuators,'' in Proc.IEEE Int. Workshop on Intelligent Robots and Systems (IROS'95), Pittsburg, USA, 1995, pp. 399–406.*

[6] *A. D. Luca, F. Flacco, A. Bicchi, and R. Schiavi, "Nonlinear decoupled motion-stiffness control and collision detection/reaction for the vsa-ii variable stiffness device," in IEEE Int. Conf. on Intelligent Robotic Systems, 2009.*

[7] *S. Haddadin, A. Albu-Sch¨affer, and G. Hirzinger, "Safety evaluation of physical human-robot interaction via crash-testing," in Robotics: Science and Systems Conference (RSS2007), 2007.*

[8] *K. Koganezawa, T. Inaba, and T. Nakazawa, ''Stiffness and angle control of antagonistially driven joint,'' in Proc. 1st IEEE/RAS-EMBS Int. Conf. Biomedical Robotics and Biomechatronics (BioRob'06), 2006, pp. 1007–1013.*

[9] *S. A. Migliore, E. A. Brown, and S. P. DeWeerth, "Biologically Inspired Joint Stiffness Control," in IEEE Int. Conf. on Robotics and Automation (ICRA2005), Barcelona, Spain, 2005.*

[10] *R. Kolacinski and R. Quinn, ''Design and mechanics of an antagonistic biomimetic actuator system,'' in Proc. 1998 IEEE Int. Conf. Robotics and Automation, 1998, vol. 2, pp. 1629–1634.*

[11] *G. Tonietti, R. Schiavi, and A. Bicchi, "Design and control of a variable stiffness actuator for safe and fast physical human/robot interaction," in Proc. 2005 IEEE International Conference on Robotics and Automation. Interdepartmental Research Center E. Piaggio Faculty of Engineering, University of Pisa via Diotisalvi,2 56100, Pisa (Italy): IEEE, April 2005, pp. 582–533.*

[12] *R. Horst and R. Marcus, ''Flexcva: A continuously variable actuator for active orthotics,'' in 28th Proc. Annu. Int. Conf. IEEE Engineering in Medicine and Biology Society (EMBS'06), 2006, vol. 1, pp. 2425–2428.*

[13] *C. English and D. Russell, ''Mechanics and stiffness limitations of a variable stiffness actuator for use in prosthetic limbs,'' Mechanism Mach. Theor., vol. 34, no. 1, pp. 7–25, Jan. 1999.*

[14] *S. Kota, J. Hetrick, Z. Li, L. Saggere. 'Tailoring Unconventional Actuators with Compliant Transmissions: Design Methods and Applications'. IEEE/ASME Transactions on Mechatronics, Vol. 4, No. 4 December 1999 pp396-408.*

[15] *Ananthasuresh G. K., Kota S., 'Designing Compliant Mechanisms'. ASME Mechanical Engineering, November 1995.*

[16] *Saggere, L., Kota S. 'Static Shape Control of Smart Structures Using Compliant Mechanisms'. AIAA Journal, Volume 37, Number 5, pp.572-578, May 1999.*

[17] *X. Lachenal, P. M. Weaver, S. Daynes. Multistable composite twisting structure for morphing applications. Proceedings of the Royal Society A: Mathematical, Physical and Engineering Science 2012; 468: 21. DOI: 10.1098/rspa.2011.0631.*

[18] *A. Pirrera 'Bistable Structures for Morphing Applications Using Anisotropic Shells', 2011. Thesis University of Bristol*

[19] *A. Pirrera, D. Avitabile, P. M. Weaver 'Bistable plates for morphing structures: A refined analytical approach with high-order polynomials', International Journal of Solids and Structures, 47, (pp. 3412-3425), 2010*

[20] *A. Pirrera, D. Avitabile, P. M. Weaver 'On the thermally induced bistability of composite cylindrical shells for morphing structures', , International Journal of Solids and Structures, 49 (5), (pp. 685 - 700), 2012*

[21] *Kollar L. P., Springer G. S., Mechanics of composite structures. Cambridge, UK: 2003*

[22] *Jones R. M., Mechanics of composite materials. 2nd Edn ed.: London, UK: 1999.*

[23] *Calladine C. R., Theory of shell structures. Cambridge, UK: 1983.*

[24] *Hexcel, HexPly® 8552 data sheet, 2007, Hexcel.*